SUPPORTING INFORMATION

Nanoparticle-based pseudo hapten for target-responsive cargo release for magnetic mesoporous silica nanocontainer

Zhuangqiang Gao, Dianping Tang,* Mingdi Xu, Guonan Chen, and Huanghao Yang*

[a]*Ministry of Education & Fujian Provincial Key Laboratory of Analysis and Detection for Food Safety, Department of Chemistry and Chemical Engineering, Fuzhou University, Fuzhou 350108, PR China*

[b]*Institute of Environmental and Analytical Science, School of Chemistry and Chemical Engineering, Henan University, Kaifeng 475004, Henan, PR China*

E-mail: dianping.tang@fzu.edu.cn (D. Tang)

Fax: +86 591 2286 6135; Tel.: +86 591 2286 6125.

Table of Content

EXPERIMENTAL PROCESS S2
1. Materials and Reagents S2
2. Apparatus S2
3. Preparation of Magnetic Mesoporous $NiCo_2O_4$ Nanostructures (MMB) S3
4. Conjugation of MMB with Antibody (mAb-MMB) S3
5. Preparation of Poly(ethyleneimine)-capped Polystyrene Microspheres (PEI-PSMS) S4
6. Preparation of Homogeneous Immunosensing Probe (MMB-PSMS) S5
7. Immunoassay Protocol and PGM Measurement S5
PARTIAL RESULTS AND DISCUSSION S6
8. Characterization of mAb-MMB and PEI-PSMS S6
9. Optimization of Experimental Conditions S10
10. Analysis of Real Sample and Evaluation of Method Accuracy S12
11. Eliminating the Interference of Endogenous Glucose in Human Serum Sample 14
REFERENCES 16

EXPERIMENTAL PROCESS

1. Materials and Reagents

Individual standard stock samples of brevetoxin B (PbTx-2) and aflatoxin B_1 (AFB_1) were purchased from Express Technol. Co. Ltd. (Beijing, China). Monoclonal mouse anti-PbTx-2 antibody and monoclonal mouse anti-AFB_1 antibody were provided by Dingguo Biotechnol. Co. Ltd (Beijing, China). Mouse monoclonal anti-human antibody against prostate-specific antigen (anti-PSA) was purchased from Abcam Inc. (Cambridge, MA). PSA standards were obtained from Biocell Biotechnol. Co., Ltd. (Zhengzhou, China). Triblock copolymer of Pluronic (P123), and 3-aminopropyltriethoxysilane (APTES) were purchased from Sigma-Aldrich (St. Louis, MO, USA). Cobalt and nickel hydrous nitrates ($Co(NO_3)_2 \cdot 6H_2O$, $Ni(NO_3)_2 \cdot 6H_2O$), dimethylformamide (DMF), diglycolic anhydride, glutaraldehyde, *n*-butylalcohol, and tetraethoxysilane (TEOS) were purchased from Sinopharm Chem. Re. Co. Ltd. (Shanghai, China). Polyehyleneimine (PEI, branched, MW 10,000, 99 wt %) was purchased from Aldrich (Steinheim, Germany). Polystyrene microspheres (PSMS, 200 – 300 nm in diameter) were obtained from Yangzhou HuiTong Polyester Technology Co., LtD (Yangzhou, China). All other reagents were of analytical grade and were used without further purification. Ultrapure water obtained from a Millipore water purification system (≥18 MΩ, Milli-Q, Millipore) was used in all runs. Personal glucose meter (PGM) buffer (pH 7.3) was consisted of 72.9 mM Na_2HPO_4, 27.1 mM NaH_2PO_4, 50 mM NaCl and 5 mM $MgCl_2$.

2. Apparatus

The glucose meter was from Roche Diagnostics GmbH (Mannheim, Germany). The morphology of nanostructures used in this study was characterized by transmission electron microscopy (TEM) on a H-7650 (Hitachi Instrument, Japan) microscope. Scanning electron micrograph was taken with a Scanning Electron Microscope (SEM, S-4800, Hitachi, Japan). XRD patterns were recorded on a PANalytical X'Pert spectrometer using the Co Kα radiation (λ = 1.789 Å), and the data would be changed to Cu Kα data. N_2 adsorption–desorption analysis was measured on a Micromeritics ASAP 2000 instrument (Micromeritics, Norcross, GA, USA). Pore volumes were determined using the adsorbed volume at a relative pressure of 0.99. Multipoint Brunauer–Emmet–Teller (BET) surface area was estimated from the relative pressure range from 0.06 to 0.3. The pore size distributions of

the as-prepared samples were analyzed using the Barrett–Joyner–Halenda (BJH) method. Magnetic measurements were made using Nanjing University Instruments on vibrating sample magnetometer (VSM) at room temperature that produces fields of up to 6 T on the sample. Fourier transform infrared spectroscopy (FT-IR) of the bionanomaterials was characterized by FT-IR system (Spectrum GX, PerkinElmer, USA). X-ray photoelectron spectroscopy (XPS) measurements were carried out using a VG Scientific ESCALAB 250 spectrometer with Al Kα X-ray (1486.6 eV).

3. Preparation of Magnetic Mesoporous $NiCo_2O_4$ Nanostructures (MMB)

Mesoporous silica KIT-6 was prepared according to the literature.[S1] High crystalline mesoporous $NiCo_2O_4$ were successfully prepared through the nanocasting strategy, using KIT-6 as a hard template, and described in our recent report.[S2] Briefly, nickel (II) nitrate hexahydrate [$Ni(NO_3)_2{\cdot}6H_2O$] and cobalt (II) nitrate hexahydrate [$Co(NO_3)_2{\cdot}6H_2O$] (total mass: 1g) with the molar ratio of 1 : 2 were dissolved in ethanol to form a hybrid solution. After stirring at room temperature (RT) for 1 h, 0.5 g of KIT-6 was added into the mixture. The suspension was stirred until dry at RT, and the sample was then calcined at 300 °C for 3 h. This procedure was repeated twice and then calcined at 380 °C for 4 h. The silica template was removed by etching twice with 2 M NaOH aqueous solution at 60 °C for 12 h each time. After centrifuging and decanting off the clear solution, the solid was washed thrice with distilled water and ethanol, and then dried at 80 °C to obtain magnetic mesoporous $NiCo_2O_4$ nanostructures (designated as MMB). The as-prepared MMB were characterized by using different methods and technologies.

4. Conjugation of MMB with Antibody (mAb-MMB)

30 mg of MMB were initially dispersed into 2-mL ultrapure water, and then 5 μL NaOH, 10 μL APTES and 25 μL TEOS were added into the solution under stirring. The suspension was kept stirring and refluxed for 8 h at RT. Following that, the APTES-coated MMB were separated and purified by magnetic decantation. Subsequently, the resultant particles were re-dispersed in 2 mL ultrapure water containing 1 mL 25 wt % glutaraldehyde and stirred for 6 h at RT. After magnetic separation, the glutaraldehyde-functionalized MMB was dispersed in 1 mL PGM buffer (pH 7.3). Then, 180 μL (*Note*: The amount was optimized) of anti-PbTx-2 antibody (0.2 mg mL^{-1}) was added into the prepared-above suspension, and slightly shaken overnight at 4 °C. To reduce the resultant

schiff bases and any excess aldehydes, 50 μL of 25 mg mL^{-1} sodium cyanoborohydride was added to the suspension, and incubated for 1 h at 4 °C. Afterwards, the mixture was collected by applying an external magnet. The obtained pellet (*i.e.* anti-PbTx-2-conjugated MMB, designated as mAb-MMB, $C_{[MMB]} \approx 30$ mg mL^{-1}) was redispersed into 1 mL PGM buffer (pH 7.3), and stored at 4 °C until use. Scheme S1 shows the preparation process of mAb-MMB.

By the same token, the conjugates with anti-AFB_1 and anti-PSA antibody were prepared using the similar method, respectively.

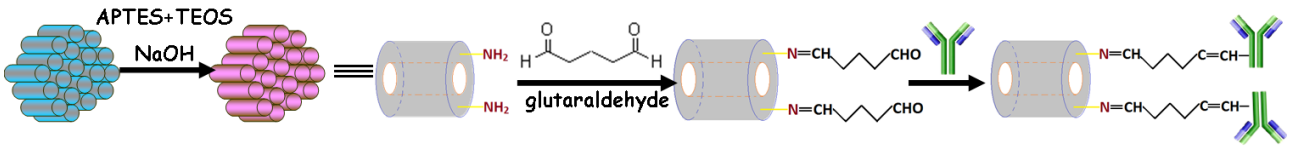

Scheme S1. Fabrication process of antibody-functionalized magnetic $NiCo_2O_4$ nanostructures.

5. Preparation of Poly(ethyleneimine)-capped Polystyrene Microspheres (PEI-PSMS)

PEI-coated polystyrene microspheres (designated as PEI-PSMS) were synthesized by using a three-step process, as described in the literature.[S3] Briefly, 30 mg of PSMS were initially dispersed into 2-mL ultrapure water, and a mixture containing 5 μL NaOH, 10 μL APTES and 25 μL TEOS were then added under stirring. The suspension was kept stirring and refluxed for 8 h at RT. Following that, the APTES-functionalized PSMS were obtained by centrifugation (*Note*: The content of nitrogen in the APTES-coated PSMS was 0.93%, estimated by element analysis). The obtained pellet was dispersed into 2 mL DMF containing 8.5 mg diglycolic anhydride. The suspension was stirred overnight at RT, and the resultant mixture was centrifuged to obtain the carboxyl-functionalized PSMS. After that, the functional PSMS and 30 mg PEI were dispersed into 4 mL ultrapure water, and stirred overnight at RT. The resulting mixture was centrifuged, washed and the obtained PEI-PSMS was dispersed into 1 mL pH 7.3 PGM buffer ($C_{[PSMS]} \approx 30$ mg mL^{-1}) (*Note*: The content of nitrogen in the PEI-PSMS was determined to be 8.12%). The results of element analysis revealed that more amino groups were coated on the surface of PEI-PSMS than that of APTES-PSMS.

6. Preparation of Homogeneous Immunosensing Probe (MMB-PSMS)

Initially, 100 μL of 30 mg mL^{-1} mAb-MMB was diluted into 1 mL pH 7.3 PGM buffer containing 350 mg glucose (optimized), and then the mixture was generally stirred 24 h at 4 ºC. During this process, partial glucose molecules were stirred into the pores. After that, 150 μL of 30 mg mL^{-1} PEI-PSMS was added into the suspension, and incubated for 2 h at 4 ºC with stirring. As a result, the positively charged PEI-PSMS were adsorbed on the surface of the negatively charged mAb-MMB, and capped on the pores. After magnetic separation and washing with PGM buffer, the obtained MMB-mAb-PEI-PSMS loading with glucose molecules (designated as MMB-PSMS) were redispersed into 150 μL PGM buffer, and used for the detection of target analyte. The fabrication procedure of MMB-PSMS is schematically illustrated in Scheme S2.

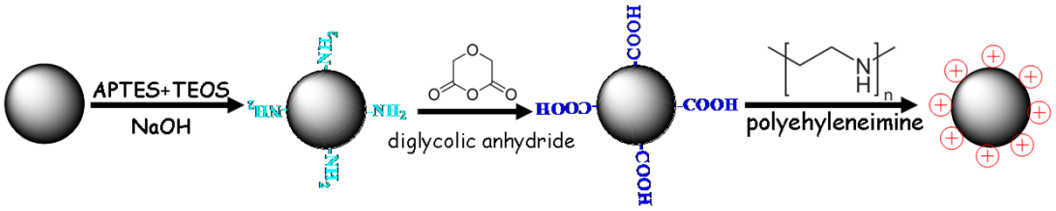

Scheme 2. Preparation process of PEI-coated olystyrene microsphere.

7. Immunoassay Protocol and PGM Measurement

10 μL of the prepared-above MMB-PSMS suspension was initially injected into 200-μL PCR tube, and PbTx-2 standards/samples with various concentrations were added into the tube. The tubes were shaken occasionally during the reaction at RT. During this process, target PbTx-2 triggered the MMB-PSMS, and displaced the PEI-PSMS from the MMB-PSMS probe due to the antigen-antibody specific reaction. Use of monoclonal antibody was conducive for the open of molecular gate, thereby resulting in the release of the entrapped glucose molecules from the pore. After incubation for 25 min, a 3-μL aliquot of the supernatant was removed for glucose measurement by using the commercialized Roche PGM. The obtained PGM signal was registered as the immunosensing signal relative to different-concentration target analytes. All measurements were carried out at room temperature (25 ± 1.0 ºC). All data were obtained with three measurements each in parallel. Scheme S3 shows the immunoreaction protocol and the release process of glucose.

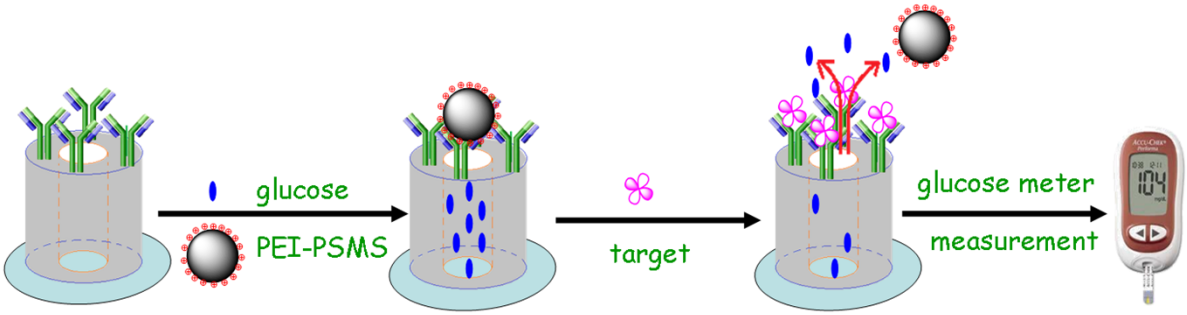

Scheme S3. PGM measurement procedure.

PARTIAL RESULTS AND DISCUSSION

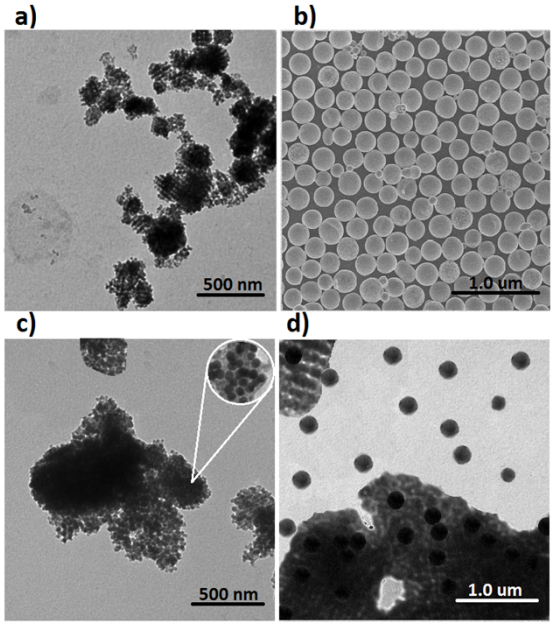

Fig. S1 TEM images of a) mAb-MMB, c) MMS-PSMS (inset, magnification image), and d) the synthesized MMB-PSMS in the presence of 1 ng mL^{-1} target PbTx-2. b) SEM image of PEI-PSMS.

8. Characterization of mAb-MMB and PEI-PSMS

During the synthesis of APTES-PSMS, we investigated the content of nitrogen by using element analysis (~ 0.93 wt % N), indicating that the amount of $–NH_2$ groups on the APTES-PSMS were relatively little. In this case, the synthesized APTES-PSMS were insufficient for conjugation of mAb-MMB. More importantly, APTES-PSMS were difficultly dispersed in the water due to a few of amino groups. In contrast, the as-synthesized PEI-PSMS contained much more amino groups (8.12 wt % N), which could provide more amino

groups (*i.e.* positively charged species) for the electrostatic interaction with mAb-MMB. Meanwhile, the PSMS with more amino groups could possess better water solubility. Hence, the synthesized PEI-PSMS were conducive for the development of the displacement-type homogeneous immunoassay. For comparison, PEG neutralized PEI-PSMS were used for the preparation of MMB-PSMS by using mAb-MMB and glucose based on the mentioned-above method. The PGM signals of mAb-MMB were assayed after interaction with differently charged PEI-PSMS. As shown in Fig. S2, use of PEG neutralized PEI-PSMS did not block the pores, and a large number of glucose molecules were released out, thus leading to a strong PGM signal in comparison with negatively charged PEI-PSMS. Fig. S3 displays the typical XRD pattern of the as-synthesized $NiCo_2O_4$ nanostructures. All the diffraction reflections could be indexed to a cubic spinel $NiCo_2O_4$ (JCPDS 073-1702), and no impurity phase was detected. [S4]

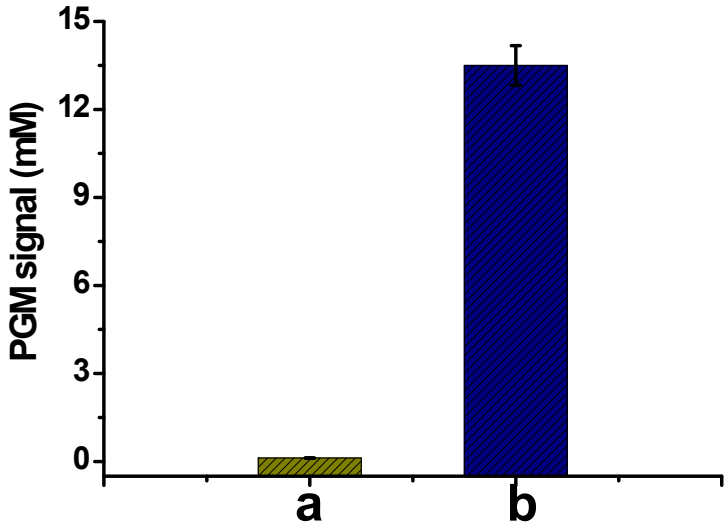

Fig. S2. The effect of using differently charged PEI-PSMS on the entrapping capacity of the guest (glucose) into the magnetic mesoporous $NiCo_2O_4$ nanostructures: a) positively charged PEI-PSMS and b) PEG neutralized PEI-PSMS.

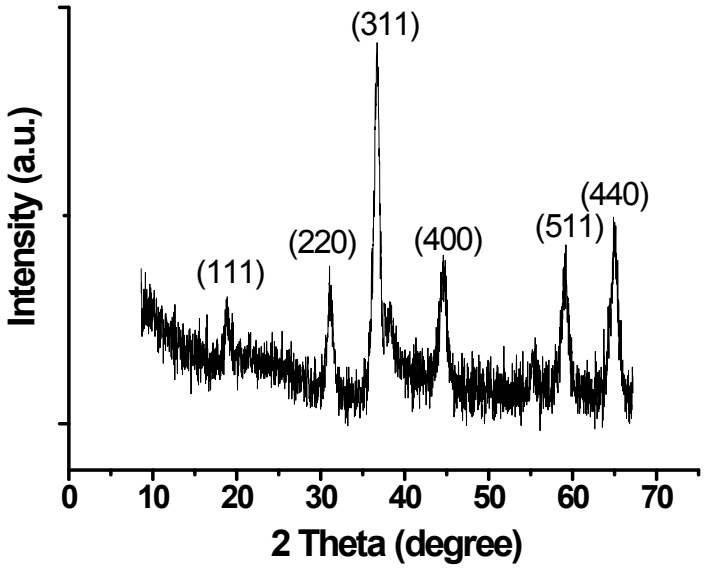

Fig. S3. Typical XRD pattern of magnetic mesoporous $NiCo_2O_4$ nanostructures.

Fig. S4 represents the Ni2p, Co2p, Si2p, O1s, N1s, and C1s core level regions of the synthesized mAb-MMB, respectively. The existence of the bands at 398.0 eV and 284.5 eV for mAb-MMB indicated the presence of N1s and C1s, which might be derived from the conjugated antibody. Type IV adsorption-desorption isotherms and H1 hysteresis loops of mAb-MMB were investigated in the range of 0 – 1.0 Pa.

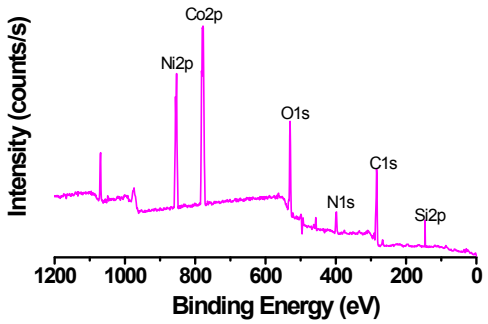

Fig. S4. XPS analysis of antibody-functionalized magnetic mesoporous $NiCo_2O_4$ nanostructures.

The nitrogen adsorption–desorption isotherm of mAb-MMB exhibits a type IV isotherm (Fig. S5), characteristic of mesoporous materials. The pore size distribution of desorption branch is depicted in the inset of Fig. S5. It clearly shows a bimodal pore size distribution for mAb-MMB, which is common in KIT-6 type mesoporous materials. The first peak at 2.9 nm can be attributed to the void space generated after the removal of silica wall, and is in good agreement with the pore size of

mesoporous silica template KIT-6, while the larger pores at 12.3 nm can be attributed to incomplete replicate in the two sets of KIT-6 templates. The specific surface area and larger pore volume of mesoporous $NiCo_2O_4$ are 133 m^2 g^{-1} and 0.52 cm^3 g^{-1}, respectively. The high surface area and relatively large pores favor the immobilization of biomolecules.

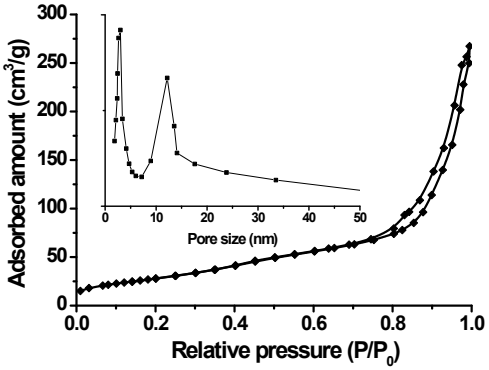

Fig. S5. Nitrogen adsorption-desorption isotherms (inset, pore size distribution) of antibody-functionalized magnetic mesoporous $NiCo_2O_4$ nanostructures.

It is well known that the shapes of the infrared absorption bands of amide I groups at 1610-1690 cm^{-1} corresponding to the C=O stretching vibration of peptide linkages and amide II groups around 1500-1600 cm^{-1} from a combination of N-H bending and C-N stretching can provide detailed information on the secondary structure of proteins.[S5] Fig. S6 represents the FT-IR spectrum of mAb-MMB. Two characteristic peaks at 1620 and 1530 cm^{-1} were appeared, which corresponded to the amide I and II groups of the antibody. The weak bands occurred in the region of 1200-1400 cm^{-1} were assigned to the wagging and twisting vibrations of the $-CH_2$ group in these proteins and were commonly referred to as the progression bands, suggesting that the antibody molecules could be conjugated onto the MMB through the chemistry conjugation method.

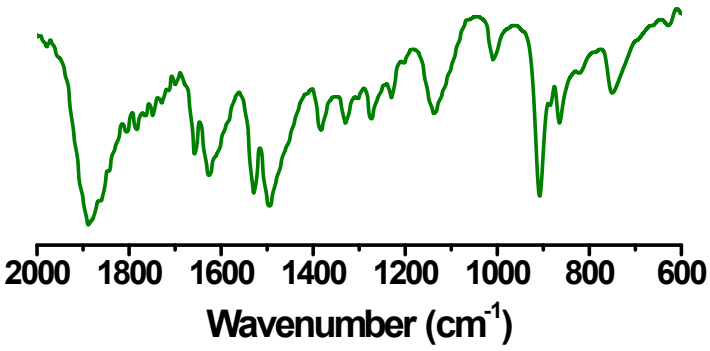

Fig. S6. FT-IR spectra of antibody-functionalized magnetic mesoporous $NiCo_2O_4$ nanostructures.

Magnetic measurements were made using Nanjing University Instruments on vibrating sample magnetometer (VSM) at room temperature that produces fields of up to 6 T on the sample. The hysteresis loops for one of the representative sample (d = 300 nm) are plotted in Fig. S7. It was found that the magnetization for MMB was 23.1 emu g^{-1}, while remanent magnetization was 15.2 emu g^{-1} for mAb-MMB. The magnetization of mAb-MMB is significantly lower as compared to MMB, indicating the biomolecules have been conjugated onto the surface of MMB. Moreover, the magnetization could still remain after modification.

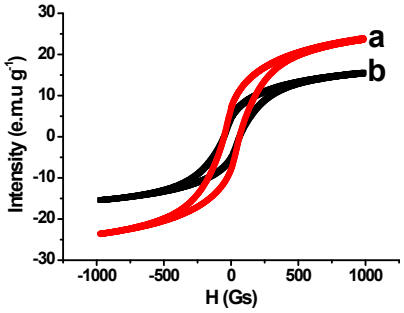

Fig. S7. VSM analysis of a) magnetic mesoporous $NiCo_2O_4$ nanostructures and b) antibody-functionalized magnetic mesoporous $NiCo_2O_4$ nanostructures.

9. Optimization of Experimental Conditions

To acquire an optimal analytical performance of the developed homogeneous immunoassay, some experimental conditions including the amount of using glucose/anti-PbTx-2/PEI-PSMS, and incubation time for the antigen-antibody reaction (*i.e.* the release time of glucose and the displacement time of target with PEI-PSMS) should be optimized. During the preparation process of MMB-PSMS, the conjugated anti-PbTx-2 antibody on the MMB acted as a gate framework (initiator). Without the immobilized antibodies around the pores, the molecular gate could not be closed. So, various-concentration anti-PbTx-2 antibodies were used for the construction of MMB-PSMS. Differently, the prepared MMB-PSMS were dissociated by using pH 4.0 PGM buffer with HCl, because the immobilized antibodies were positively charged at pH 4.0, resulting in the release of glucose. In the absence of target PbTx-2, the released glucose amount depended on the formed amount of molecular gates on the MMB. As seen from Fig. S8, an optimal amount of anti-PbTx-2

antibody was more than 180 μL (0.2 mg mL^{-1}). So, 180 μL of anti-PbTx-2 antibody (0.2 mg mL^{-1}) was selected for the conjugation of mAb-MMB in 2 mL ultrapure water containing 30 mg MMB.

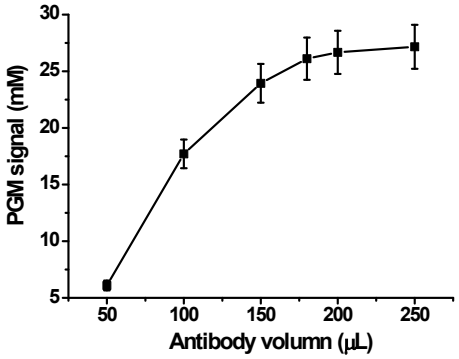

Fig. S8. The entrapping efficiency of various antibody concentrations on the PGM-based immunosensing probe.

In this work, the PGM signal mainly derived from the entrapped glucose molecules in the pores. The entrapped amount directly affected the detectable signal of the immunosensing probes. On the conditions of other excess components, we investigated the effect of various-mass glucose on the PGM signals of as-prepared MMB-PSMS (1 ng mL^{-1} PbTx-2 as an example). As seen from Fig. S9-a, the PGM signal initially increased with the increasing glucose, and then tended to level off ($\geq$ 350 mg glucose in 1 mL solution containing 100 μL of 30 mg mL^{-1} mAb-MMB). That is to say, the selected amount of glucose should be more than 350 mg. On considering the viscosity effect of using high-concentration glucose, 350 mg glucose was preferable. By the same token, the amount of PEI-PSMS (as the molecular gate) also influenced the sensitivity of the PGM-based immunosensing probe. The judgment was carried out by using 1 ng mL^{-1} PbTx-2 as an example. As indicated from Fig. S8-b, the optimized amount of PEI-PSMS was 150 μL of 30 mg mL^{-1}. Therefore, 350 mg glucose and 150 μL of 30 mg mL^{-1} PEI-PSMS used for the preparation of MMB-PSMS in 1 mL pH 7.3 PGM buffer containing 100 μL of 30 mg mL^{-1} mAb-MMB.

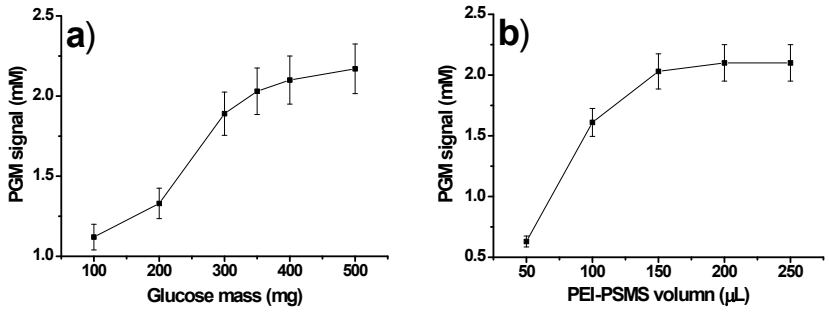

Fig. S9. The effect of a) glucose amount and b) PEI-PSMS concentration on the PGM signal of the PGM-based immunosensing probe (1 ng mL^{-1} PbTx-2 used in this case).

To achieve an adequate release of glucose from the pores, the opened number of molecular gate was very important. In this study, the molecular gates were switched on by the antigen-antibody reaction. So, we also monitored the effect of incubation time on the PGM signal of the MMB-PSMS at RT. As shown in Fig. S10, the detectable signals increased with the increment of incubation time, and tended to level off after 25 min. Hence, an incubation time of 25 min was selected for sensitive determination of target PbTx-2 at acceptable throughput.

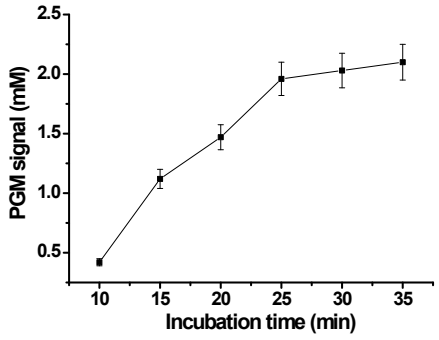

Fig. S10. The effect of incubation time for the antigen-antibody reaction on the PGM signal of the PGM-based immunosensing probe (1 ng mL^{-1} PbTx-2 used in this case).

10. Analysis of Real Sample and Evaluation of Method Accuracy

To monitor the analytical reliability and potential applicability of the PGM-based immunoassay for testing real samples, 15 spiked seafood samples with different-concentration PbTx-2, such as *Sinonovacula constricta, Musculista senhousia* and *Tegillarca granosa*, were assessed by using the PGM-based immunoassay and commercialized PbTx-2 ELISA kit (Abraxis LLC, Warminster, USA) as a reference method. Mollusk standards were prepared as follows: Seafood samples including *Musculista senhousia*, *Sinonovacula constricta*, and *Tegillarca granosa* were purchased from the local Carrefour supermarket (Fuzhou, China). 5 g of minced sample tissue was initially placed in a centrifuge tube, then 20 mL of dimethyl sulfoxide (50%, w/v) was added, and then the mixture was centrifuged for 10 min at 2,500 g. The resulting supernatant was passed sequentially through a 100-nm nylon mesh, no. 1 filter and a GF/B filter (Whatman) in turn (*Note*: The extract color was slightly opalescent yellow). Following that, PbTx-2 standards with various levels were

spiked into the supernatant, respectively. The assayed results using two methods are listed in Table S1. Comparison of the experimental results obtained with the proposed immunoassay with those of ELISA was performed via the use of a least-squares regression method. The regression line was fitted to $y = 0.9802x + 0.1004$ ($R^2 = 0.9921$, $n = 36$; x represents the assay results of using the PGM-based immunosensing probe while y is the results of using the commercialized PbTx-2 ELISA kit). The standard deviations of the slope and intercept are given on the regression equation. The correlation between the two methods was investigated using *t*-tests for comparison of the experimental values of the intercept and slope to the ideal situation of zero intercept and slope of 1. The statistics t for the slope and intercept were calculated respectively as follows: $t = (b-1)/s_b$ and $t = (a-0)/s_a$ where b and a stands for the slope and intercept, respectively, and s_b and s_a for the standard deviation of the slope and intercept, respectively. No significance differences at the 0.05 significance level were encountered between the optimum values of intercept and slope and experimental data, thereby revealing a good agreement between both analytical methods.

Importantly, an uncontaminated sample was estimated as negative. Because of sample dilution in the extraction protocol, as described under Experimental, 3 samples were detected as negatives in the ELISA.

Table S1. Comparison of the assay results for real samples using the PGM-based immunoassay and the commericalized PbTx-2 ELISA kit.

	method; concentration (mean ± SD, ng mL^{-1}, $n = 3$)[a]		
Sample[c]	PGM-based immunoassay	ELISA	RSD (%)
1	-[c]	-[c]	-
2	0.47	0.51	5.7
3	1.43	1.57	6.6
4	8.76	8.46	2.5
5	15.2	14.3	4.3
6	-[c]	-[c]	-
7	0.51	0.47	5.8
8	1.52	1.61	4.1
9	9.12	8.72	3.2
10	14.5	15.6	5.2
11	-[c]	-[c]	-

12	0.49	0.54	6.9
13	1.48	1.58	4.6
14	8.72	9.32	4.7
15	14.9	14.1	3.9

[a]The mean value of three assays (n = 3), and the regression equation (linear) for these data is as follows: $y = 0.9802x + 0.1004$ (R^2 = 0.9921, n = 36; x represents the assay results of using the PGM-based immunosensing probe while y is the results of using the commercialized PbTx-2 ELISA kit). [b]Samples 1−5, 6−10, and 11−15 were used as *S. constricta*, *M. senhousia*, and *T. granosa* supernatants as matrices, respectively. Samples 1, 6, and 11 were the unspiked specimens. These samples were made available as the extract supernatant using the sample preparation described in the Experimental Procedures. [c]The symbol "–" suggested that the sample could not be assayed by the corresponding method.

11. Eliminating the Interference of Endogenous Glucose in Human Serum Sample

Logically, another concern arises as to whether the PGM-based immunoassay system could be applied for the determination of biomarkers in human serum containing a certain amount of endogenous glucose. Actually, due to the presence of endogenous glucose in human serum, it might interfere with the final assay results. To tackle this problem, the glucose concentration in an unknown sample must be monitored using the PGM prior to target detection. When the background signal plus the signal generated by the target analyte exceeds the upper limit of the PGM readout, however, an appreciate dilution should be preferable. In this case, the background signal can be subtracted from the signal obtained in the subsequent actual test. To demonstrate this point, PSA was used as a model. Initially, mouse anti-human PSA antibody was conjugated onto the magnetic mesoporous $NiCo_2O_4$ nanostructures by using the mentioned-above method. Following that, PSA samples with various concentrations were assayed by using the PGM-based immunoassay protocol. In this experiment, five PSA standards with various concentrations were determined by using the PGM-based immunoassay in the presence of 0, 1 mM and 30 mM glucose, respectively (*Note*: The assay range of the PGM is 0.6 – 33.3 mM glucose). For containing 1-mM glucose PSA samples, we directly used the subtracted method. For 30-mM glucose samples, they were initially diluted by using PGM buffer, and then assayed. The real content of PSA in these samples were obtained by using the obtained-above calibration curve. The results were compared with those of using commercialized PSA ELISA kit (Biocell, Zhengzhou, China). The results are shown in Fig. S11. As indicated from Fig. S11, the results of PSA detection in the samples containing different-level glucose after pretreatments were comparable to those in the glucose-free samples. Therefore, the

pretreatment for glucose-containing samples was reliable for successfully eliminating glucose interference.

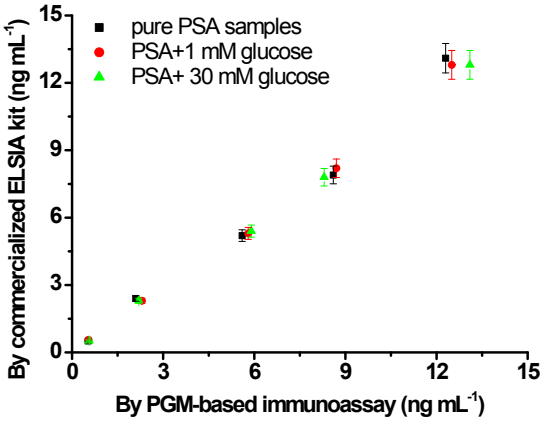

Fig. S11. Comparison of the assayed results for PSA samples in the absence and presence of various-concentration glucose by using the PGM-based immunoassay and commercialized PSA ELISA kit.

REFERENCES

[S1] Zhao, D.; Huo, Q.; Feng, J.; Chmelka, B.; Stucky, G. Nonionic triblock and star diblock copolymer and oligomeric surfactant syntheses of highly ordered, hydrothermally stable mesoporous silica structures. *J. Am. Chem. Soc.* **1998**, *120*, 6024-6036.

[S2] Li, Q.; Zeng, L.; Wang, J.; Tang, D.; Liu, B.; Chen, G.; Wei, M. Magnetic mesoporous organic-inorganic $NiCo_2O_4$ hybrid nanomaterials for electrochemical immunosensors. *ACS Appl. Mater. Interfaces* **2011**, *3*, 1366-1373.

[S3] le Masne de Chermont, Q.; Chaneac, C.; Seguin, J.; Pelle, F.; Maitrejean, S.; Jolivet, J.; Gourier, D.; Bessodes, M.; Schermen, D. Nanoprobes with near-infrared persistent luminescence for *in vivo* imaging. *Proc. Natl. Acad. Sci. USA* **2007**, *104*, 9266-8271.

[S4] Yang, P.; Zhao, D.; Margolese, D.; Chmelka, B.; Stucky, G. Generalized syntheses of large-pore mesoporous metal oxides with semicrystalline frameworks. *Nature* **1998**, *396*, 162-155.

[S5] Tang, D.; Yuan, R.; Chai, Y. Electrochemical immuno-bioanalysis for carcinoma antigen 125 based on thionine and gold nanoparticles modified carbon paste interface. *Anal. Chim. Acta* **2006**, *564*, 158-165.